Engineering Science and Technology, an International Journal xxx (2016) xxx–xxx

HOSTED BY

ELSEVIER

Contents lists available at ScienceDirect

Engineering Science and Technology, an International Journal

journal homepage: www.elsevier.com/locate/jestch

Full Length Article

Experimental investigation on low-frequency vibration assisted micro-WEDM of Inconel 718

Deepak Rajendra Unune *, Harlal Singh Mali

Mechanical Engineering Department, Malaviya National Institute of Technology, Jaipur 302017, Rajasthan, India

ARTICLE INFO

Article history:
Received 16 April 2016
Revised 17 June 2016
Accepted 24 June 2016
Available online xxxx

Keywords:
Micro-wire electric discharge machining
Low-frequency
Vibration
Micro-channels
Surface quality
MRR
Kerf

ABSTRACT

The micro-wire electric discharge machining (micro-WEDM) has emerged as the popular micromachining processes for fabrication of micro-features. However, the low machining rate and poor surface finish are restricting wide applications of this process. Therefore, in this study, an attempt was made to improve machining rate of micro-WEDM with low-frequency workpiece vibration assistance. The gap voltage, capacitance, feed rate and vibrational frequency were chosen as control factors, whereas, the material removal rate (MRR) and kerf width were selected as performance measures while fabricating microchannels in Inconel 718. It was observed that in micro-WEDM, the capacitance is the most significant factor affecting both MRR and kerf width. It was witnessed that the low-frequency workpiece vibration improves the performance of micro-WEDM by improving the MRR due to enhanced flushing conditions and reduced electrode-workpiece adhesion.

1. Introduction

The Nickel-based superalloys find widespread application in aerospace, automobile, medical, and chemical industries owing to their excellent resistivity to corrosion and oxidation, high creep-rupture strength, and fatigue endurance limit. Among Nickel-based superalloys, Inconel 718 is largely used in the aerospace segment for fabricating of gas turbine engine components such as turbine disks, blades, combustors and casings, nuclear power plant components such as reactor and pump, spacecraft structural components, medical devices, food processing equipment, extrusion dies and containers, casting dies, hot work tools and dies, etc. [1,2]. However, Inconel-718 pose a substantial difficulties during traditional machining because of its small thermal conductivity, high work hardening characteristic, hot-hardness, chemical affection to tool material [1,3–5]. Hence, non-traditional machining processes are favored over traditional processes while machining of Inconel 718.

Wire electrical discharge machining (WEDM) is one of the important and widely used non-traditional, thermoelectric processes in manufacturing industries owing to its capability to machine intricate and free forms with very thin wires [6,7]. The physical behavior and working principle of WEDM process is well defined in the literature [8–10]. In last decade, micro-WEDM, which is a variant of WEDM, has evolved as a competent technique for machining and fabrication of micro-features in such difficult-to-cut materials regardless of their hardness. In micro-WEDM, small pulse energies are predominant, and constantly moving wire (diameter 25–150 μm) are required as tool-electrode. With benefits such as high machining efficiency, precision, and low cost, micro-WEDM gets upper-hand over the other micro-machining processes and has been extensively used in aerospace and nuclear space industry for machining of difficult-to-cut materials [11,12].

Numerous research studies have been reported on machining of conductive materials including metals, composites, ceramics, and metal matrix composites using WEDM over last two decades. In general, the machining performance of WEDM is mainly influenced by a combination of electrical, mechanical, physical, and geometrical properties of the wire electrode, properties of the workpiece material, mechanical machine concept, machine intelligence, pulse generator technology, and dielectric flushing method. Mahapatra and Patnaik [8] have investigated the effects of various parameters including discharge current, pulse duration, pulse frequency, wire speeds, wire tension, and dielectric flow rate on metal removal rate (MRR), surface finish (SF) and cutting width (kerf). They used a genetic algorithm for multi-objective optimization of WEDM.

* Corresponding author at: Mechanical Engineering Department, Malaviya National Institute of Technology, Malaviyanagar, Jaipur 302017, Rajasthan, India. Mobile: +91 8947965681.

E-mail addresses: deepununne@gmail.com (D.R. Unune), harlal.singh@gmail.com (H.S. Mali).

Peer review under responsibility of Karabuk University.

http://dx.doi.org/10.1016/j.jestch.2016.06.010
2215-0986/

Please cite this article in press as: D.R. Unune, H.S. Mali, Experimental investigation on low-frequency vibration assisted micro-WEDM of Inconel 718, Eng. Sci. Tech., Int. J. (2016), http://dx.doi.org/10.1016/j.jestch.2016.06.010

Authors of [13] used non-dominated sorting genetic algorithm-II (NSGA-II) to determine optimum process parameters in WEDM of AISI D3 for cutting rate and surface roughness. Kumar and Agrawal [14] optimized WEDM process parameter while machining high-speed steel with zinc-coated wire. They applied NSGA-II optimization technique for multi-objective optimization of cutting rate and surface finish.

The machining of titanium alloys, composites using WEDM has also been reported in the literature. Kuriakose et al. [15] machined Ti-6Al-4V titanium alloy using zinc-coated brass wire and applied machine learning-based data mining approach to study the effect of various process parameters on the cutting speed and surface finish. Machining and optimization of γ-titanium aluminide alloy have been reported in [16]. They used constrained optimization and Pareto optimization algorithm for parametric optimization of WEDM for the cutting speed, surface finish, and dimensional deviation. Manna and Bhattacharya [17] machined aluminium-reinforced silicon carbide metal matrix composite using WEDM and determined optimum machining condition by Gauss elimination dual response method. Patil and Brahmankar [18] examined the effect of WEDM parameters on surface finish, cutting speed, and kerf width using Taguchi's method while machining alumina particulate reinforced aluminum matrix composites (Al/Al2O3p) with coated brass wire material. Bobbili et al. [19] presented machining of armor materials such as aluminum alloy 7017 and rolled homogeneous armor (RHA) steel using WEDM. They further extended this work presenting multi-objective optimization of process parameters [20].

Recently, various studies have been reported [21–23] explaining the effect of different process parameters on the response measures of micro-WEDM. Han et al. [21] established a 3-D temperature and stress distribution in micro-WEDM numerically. Das and Joshi [22] have developed a mathematical model for micro-WEDM considering plasma features, moving heat source characteristics, multi-spark phenomenon, and wire vibration effect to predict the cathode erosion rate. The effects of RC-circuit process parameters on micro-WEDM performance were explained by [23]. They established mathematical models to predict the performance measures and confirmed experimentally.

Very few studies are reported on machining of Nickel-based superalloys like Inconel 718 using WEDM. The superior properties of Inconel 718, like high resistivity to corrosion and high temperature resistant, makes it competent for elevated temperature application [5,24]. Goswami and Kumar [25] investigated and optimized the input process parameters of WEDM while machining Nimonic 80A superalloy. Hewidy et al. [26] established a mathematical relationship between WEDM process parameter and performance measure viz. MRR, wear ratio, and surface roughness based on the response surface methodology in WEDM of Inconel 601 using copper wire. Ramakrishnan and Karunamoorthy [27,28] predicted the performance of WEDM of Inconel 718 using the artificial neural network. Further, they optimized MRR and surface roughness using multi-response optimization. Agrawal et al. [2] presented empirical modeling of WEDM process parameters for Inconel 718 using response surface methodology (RSM). They optimized the process performance using desirability function approach. Recently, Nayak and Mahapatra [29] presented optimization of process parameters of WEDM during machining of cryo-treated Inconel 718. It is also noticed that no study is available which reports the micro-WEDM of Inconel 718 superalloy.

The application of low-frequency workpiece vibration in micro-EDM processes has resulted in improved machining performance due to enhanced flushing conditions and reduced unstable machining conditions [30–33]. Jahan et al. [30,31] evaluated low-frequency vibration assisted μ-ED drilling of tungsten carbide and claimed that low-frequency vibration has a considerable effect on both the machining characteristics and micro-hole accuracy parameters. Recently, Lee et al. [32] concluded that low-frequency workpiece vibration (10–70 Hz) during the μ-ED drilling results in reduced machining time by 70% related to that of machining without vibration at non-rotating electrode condition. The applications of μ-WEDM are still limited owing to low machining rate of the process. No study is reported on the application of low-frequency workpiece vibration in the μ-WEDM process. Therefore, an attempt is made to improve the performance of μ-WEDM with a low-frequency workpiece vibration assistance. The gap voltage, capacitance, wire feed rate, and vibration frequency are selected as input parameters while MRR and kerf are chosen as performance measures.

2. Materials and methods

2.1. Materials

The workpiece specimen of size 27 mm × 10 mm × 2.5 mm is prepared out of commercially available Inconel 718 by using a high-speed diamond cutter (Isomet 4000 Buehler). Semiautomatic polishing machine (MetaServ® 250 Buehler) is used for polishing and grounding of workpiece specimen. The composition of the prepared Inconel 718 specimen was determined using an optical spectrometer (LECO GDS500A) which was found to be 54.4% Ni, 0.04% C, 0.084% Si, 0.06% Mn, 0.001% P, 18.8% Cr, 8.84% Fe, 13.3% Mo, 0.085 V, 2.78% Nb, 0.259%W, 0.259 Co, 0.814% Ti, 0.194% Al, 0.078% Zr. A cylindrical zinc coated brass wire (diameter 70 μm) was used as a tool electrode. The commercial "TOTAL DIEL7500IN" dielectric fluid was used as dielectric oil due to its high flash point, and high dielectric strength.

2.2. Experimentation

Mikrotools DT110 integrated multi-process micromachining tool working on the RC-pulse generator with a positional accuracy of 0.1 μm was used to perform the micro-WEDM experiments. The positive workpiece polarity was chosen as it leads to more material removal from the workpiece as compared to negative polarity electrode. The schematic representation of vibration-assisted micro-WEDM setup is shown in Fig. 1. The photograph of the experimental setup is shown in Fig. 2. The vibration device provided along with the machine tool works on the electromagnetic actuation principle and is capable of generating low-frequency vibration within 0–100 Hz. A power transistor switch supplies the periodic power supply to the electromagnet, and the control

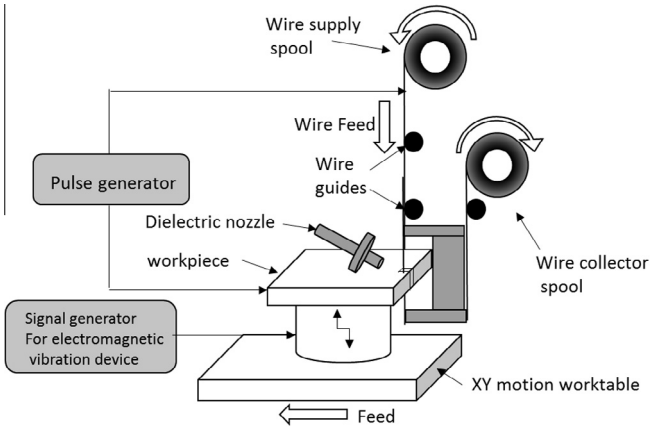

Fig. 1. Schematic diagram of vibration assisted micro-WEDM.

Please cite this article in press as: D.R. Unune, H.S. Mali, Experimental investigation on low-frequency vibration assisted micro-WEDM of Inconel 718, Eng. Sci. Tech., Int. J. (2016), http://dx.doi.org/10.1016/j.jestch.2016.06.010

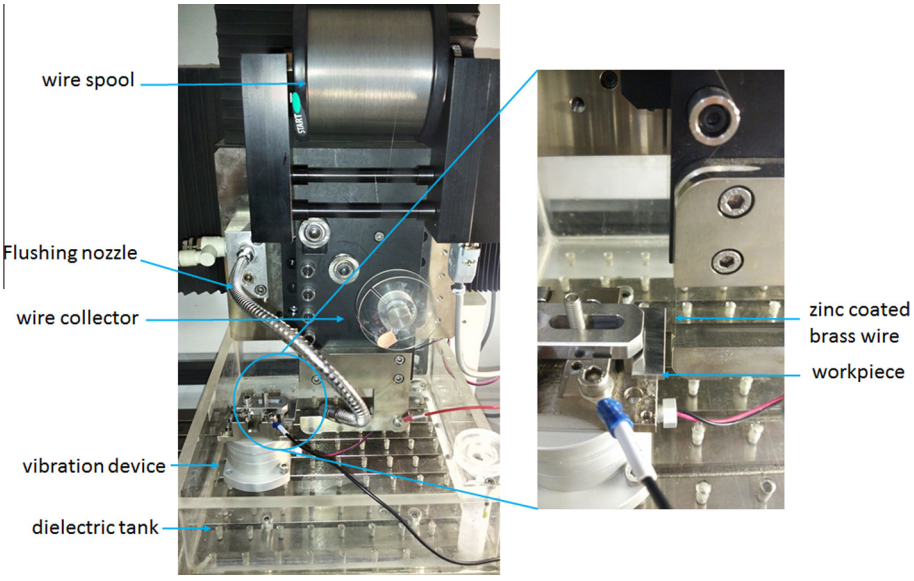

Fig. 2. Experimental setup of vibration assisted micro-WEDM.

of the on–off sequence of the power transistor is maintained using a frequency controlled pulse generator. The on–off sequence of electricity flowing through the circuit energize or de-energize the electromagnet producing the vibration. The workpiece fixture was mounted on vibration device, and vibration device was clamped inside the main EDM tank.

The Box–Behnken design was utilized to plan the experiments and total 29 runs corresponding to 24 runs for side points, and five runs replicating the center position. The gap voltage (A), capacitance (B), feed rate (C), and vibrational frequency (D) were designated as control factors while MRR and kerf width were chosen as performance measures. The control factors and their range, shown in Table 1, were decided based on the literature, trial experiments, and machine tools constraints. The experimental plan showing a set of the control factors and resultant performance measures acquired after conducting tests are given in Table 2.

2.3. Measurements

The kerf width was measured using AxioCam software and the Digital Microscope (Zeiss AxioCam AX10). The kerf width measured at five location along the length of the microchannel (as shown in Fig. 3) and then average of these measurements was considered for result analysis. The FESEM (Nova NanoSEM 450) was used to capture the microscopic images of selected machined surfaces. The weight difference of workpiece specimen before and after machining is divided by machining time to calculate MRR. The Citizon CY104 Analytical Balance (make: GMI Inc, USA) with ±0.1 mg readability and repeatability was used to measure the weight measurements. The MRR was computed using following equation:

$$\mathrm{MRR} = \frac{\nabla M_{\mathrm{wp}}}{t}\left(\frac{\mathrm{mg}}{\mathrm{min}}\right) \tag{1}$$

where, ∇M_{wp} is the weight difference before and after μ-ED milling.

Table 1
Process parameters and their levels.

	Control factors		Level		
	Symbol	Unit	−1	0	1
Gap voltage	*A*	V	80	105	130
Capacitance	*B*	μF	0.01	0.1	0.4
Feed rate	*C*	mm/min	0.1	0.25	0.4
Vibrational frequency	*D*	Hz	0	40	80

3. Results and discussion

3.1. Empirical models for performance measures

Mathematical relationships among the control factors and performance measures are established by developing multivariable regression models. The statistical significance of developed models was examined using analysis of variance (ANOVA) test. The models were improved through backward elimination method. The results of ANOVA for MRR and kerf width are summarized in Tables 3 and 4 respectively.

Fig. 4 shows the normal probability plot of the residuals which indicate that residual fall in a straight line signifying that errors are normally distributed [2]. It can also be seen that the actual response values are in good agreement with predicted values by the models (Fig. 5).

The model *F* values of 23.80_{MRR}, 95.69_{kerf} for MRR and kerf width respectively, with its Prob > *F* value less than 0.0001 directs that the models are significant. There is only a 0.01% chance that such a large model F values could occur due to noise. The values of Prob > *F* less than 0.05 indicates the significance of model terms [2,12]. For MRR, the significant model are A, B, C, D, AC, CD, and A^2 are terms contributing 2.70%, 26.38%, 24.45%, 10.88%, 3.60%, 3.55%, and 22.33%, respectively. While, A, B, B^2, and D^2 are significant model terms for kerf width contributing 7.78%, 87.47%, 8.19%, and 0.67%, respectively. The lack-of-fit values point out its significance or non-significance related to the pure error. When lack-of-fit values are non-significant, it shows that the model fits well with the experimental data. The lack-of-fit values for were found to be 0.078 and 0.1638 for MRR, and kerf width, respectively, indicating that developed models for MRR and kerf width are adequate and satisfactory.

Please cite this article in press as: D.R. Unune, H.S. Mali, Experimental investigation on low-frequency vibration assisted micro-WEDM of Inconel 718, Eng. Sci. Tech., Int. J. (2016), http://dx.doi.org/10.1016/j.jestch.2016.06.010

Table 2
Box–Behnken experimental design matrix and experimental result of performance measures.

Run order	Control factors (actual value)				Performance measures	
	Voltage (V)	Capacitance (μF)	Feed rate (mm/min)	Vibrational frequency (Hz)	MRR (mg/min)	Kerf width (μm)
1	105	0.1	0.25	40	0.0018419	124
2	105	0.1	0.25	40	0.001614	122
3	80	0.1	0.25	0	0.0034219	111
4	80	0.1	0.1	40	0.0039816	109
5	105	0.1	0.25	40	0.0017184	122
6	105	0.1	0.4	80	0.0057949	121
7	130	0.1	0.4	40	0.0038141	128
8	105	0.01	0.4	40	0.0044165	97
9	130	0.4	0.25	40	0.0019602	153
10	130	0.01	0.25	40	0.0014195	98
11	80	0.1	0.25	80	0.0057769	113
12	105	0.01	0.25	80	0.0030686	98
13	130	0.1	0.1	40	0.00096802	135
14	105	0.1	0.1	0	0.0011712	123
15	105	0.01	0.1	40	0.00097308	98
16	80	0.01	0.25	40	0.0043808	95
17	105	0.1	0.25	40	0.001496	118
18	105	0.4	0.1	40	0.0030452	147
19	130	0.1	0.25	0	0.0012259	128
20	105	0.1	0.25	40	0.00121256	120
21	105	0.1	0.1	80	0.0018346	129
22	130	0.1	0.25	80	0.0019451	134
23	80	0.4	0.25	40	0.0060939	145
24	105	0.4	0.25	0	0.0036114	155
25	105	0.01	0.25	0	0.0016407	101
26	80	0.1	0.4	40	0.0060397	109
27	105	0.4	0.4	40	0.0061797	151
28	105	0.4	0.25	80	0.0060655	153
29	105	0.1	0.4	0	0.0036652	129

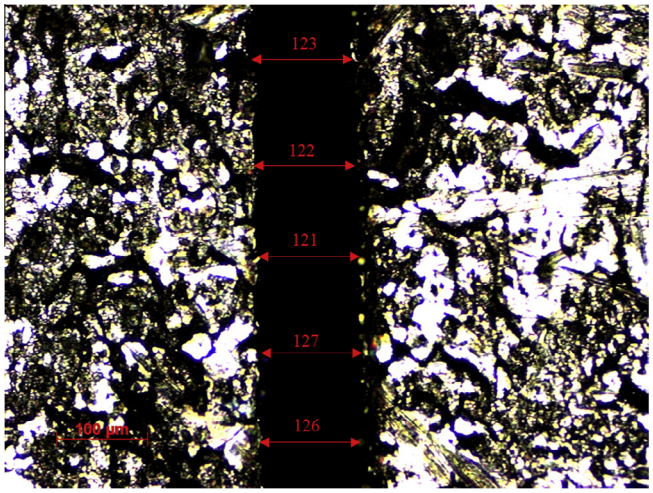

Fig. 3. Measurement of kerf width using optical microscope.

The adequacy of model fit can be described with a determination coefficient (R^2). The R^2 values for MRR and kerf width are found to be 0.9049, and 0.9696, respectively suggesting that developed models are adequate in representing the process. The other R^2 statistics, the Pred R^2 values (0.7243_{MRR}, 0.9423_{kerf}) are in agreement with the Adj R^2 (0.8669_{MRR}, 0.9595_{kerf}). The coefficient of variation (C.V.) values (23.39_{MRR}, 3.03kerf) directs higher accuracy and consistency of the performed experiments [28]. The Adeq Precision values, which signifies that signal-to-noise ratio, found to be 18.046_{MRR} and 35.102_{kerf} which are more than desired value of 4 and thus specifies a sufficient signal for the model. Therefore, developed models can be used to navigate within the design space.

The regression models for performance measures MRR and kerf width are given by second order polynomial Eqs. (2) and (3) respectively:

$$\begin{aligned}\text{MRR} = {} & -0.22818 + (5.15586 \times 10^{-4})\text{A} + (6.4794 \times 10^{-3})\text{B} \\ & - (0.032039)\text{C} - (1.42332 \times 10^{-5})\text{D} + (2.32532 \times 10^{-4})\text{AD} \\ & + (1.44429 \times 10^{-4})\text{CD} - 2.6488B^2 + 0.021177\text{C}^2 \end{aligned} \quad (2)$$

$$\begin{aligned}\text{Kerf width} = {} & +58.55654 + 0.31572\text{A} + 310.69223\text{B} \\ & + 19.95333\text{C} - (-4.47727 \times 10^{-3})\text{D} - 0.58333\text{CD} \\ & - 426.95416\text{B}^2 + (1.91534 \times 10^{-3})\text{D}^2 \end{aligned} \quad (3)$$

3.2. Analysis for MRR

The perturbation plot showing effects of control factors on MRR in micro-WEDM of Inconel 718 is shown in Fig. 6. A sharp slope for gap voltage (A), capacitance (B), feed rate (C), and vibrational frequency (D) directs that the MRR is highly sensitive to these factors. It is evident from the Table 3 that the interactions which significantly contributes to the MRR are those between the voltage and feed rate 'AC', and feed rate and vibrational frequency 'CD'. It is observed that MRR increases with increases linearly with increase in capacitance, feed rate, and vibrational frequency values. However, MRR increases initially with an increase in gap voltage up to an optimum value of 105V and then decreases with further increase in gap voltage (see, Figs. 6 and 7(a)). The discharge energy (DE) engendered in RC pulse circuit is a multiplication of capacitance and voltage (DE = 0.5 * Capacitance * Voltage^2). When the voltage values reaches the breakdown voltage value, the DE stored

Please cite this article in press as: D.R. Unune, H.S. Mali, Experimental investigation on low-frequency vibration assisted micro-WEDM of Inconel 718, Eng. Sci. Tech., Int. J. (2016), http://dx.doi.org/10.1016/j.jestch.2016.06.010

Table 3
The ANOVA table for MRR.

Source	Sum of square	df	Mean square	*F* value	*p*-Value Prob > *F*	
Model	8.452E−005	8	1.056E−005	23.80	<0.0001	Significant
A-Voltage	2.286E−006	1	2.286E−006	5.15	0.0345	
B-Capacitance	2.227E−005	1	2.227E−005	50.17	<0.0001	
C-Feed rate	2.064E−005	1	2.064E−005	46.48	<0.0001	
D-Vibration Frequency	9.187E−006	1	9.187E−006	20.69	0.0002	
AC	3.042E−006	1	3.042E−006	6.85	0.0165	
CD	3.004E−006	1	3.004E−006	6.77	0.0171	
A^2	1.885E−005	1	1.885E−005	42.45	<0.0001	
C^2	1.561E−006	1	1.561E−006	3.52	0.0754	
Residual	8.880E−006	20	4.440E−007			
Lack of Fit	8.412E−006	16	5.258E−007	4.50	0.0780	Not significant
Pure Error	4.675E−007	4	1.169E−007			
Cor Total	9.340E−005	28				
	Std. Dev.		6.663E−004	R-squared		0.9049
	Mean:		2.849E−003	Adj R-squared		0.8669
	C.V.%		23.39	Pred R-squared		0.7243
	PRESS		2.575E−005	Adeq precision		18.046

Table 4
The ANOVA table for Kerf width.

Source	Sum of square	df	Mean square	*F* value	*p*-value Prob > *F*	
Model	9296.91	7	1328.13	95.69	<0.0001	Significant
A-Voltage	747.59	1	747.59	53.86	<0.0001	
B-capacitance	8395.23	1	8395.23	604.85	<0.0001	
C-feed rate	3.08	1	3.08	0.22	0.6422	
D-vibration frequency	0.16	1	0.16	0.012	0.9146	
CD	49.00	1	49.00	3.53	0.0742	
B^2	786.10	1	786.10	56.64	<0.0001	
D^2	64.82	1	64.82	4.67	0.0424	
Residual	291.48	21	13.88			
Lack of fit	268.94	17	15.82	2.81	0.1638	Not significant
Pure error	22.54	4	5.63			
Cor total	9588.38	28				
	Std. Dev.		3.73	R-squared		0.9696
	Mean:		122.94	Adj R-squared		0.9595
	C.V.%		3.03	Pred R-squared		0.9423
	PRESS		553.66	Adeq precision		35.102

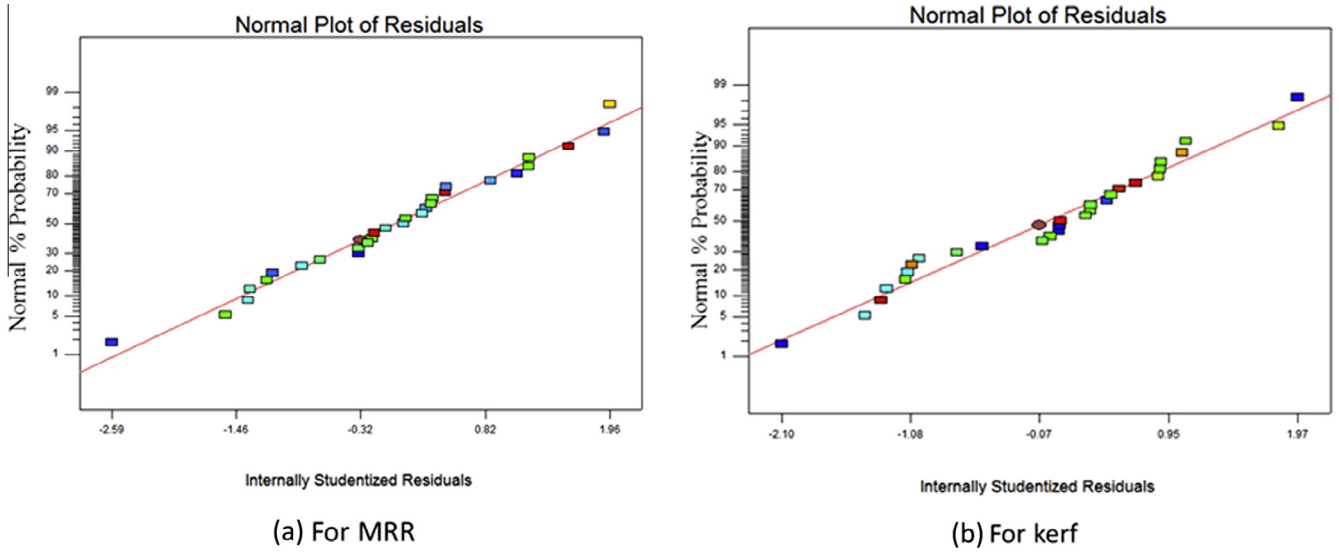

Fig. 4. Normal probability plot of residuals.

Please cite this article in press as: D.R. Unune, H.S. Mali, Experimental investigation on low-frequency vibration assisted micro-WEDM of Inconel 718, Eng. Sci. Tech., Int. J. (2016), http://dx.doi.org/10.1016/j.jestch.2016.06.010

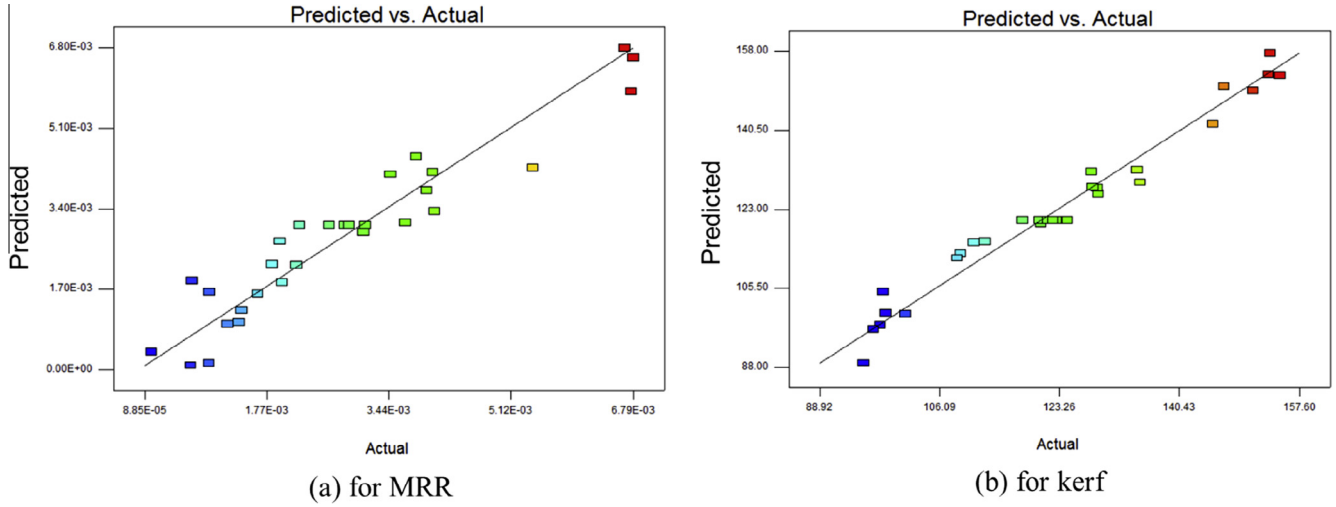

Fig. 5. Plot of predicted vs. actual response.

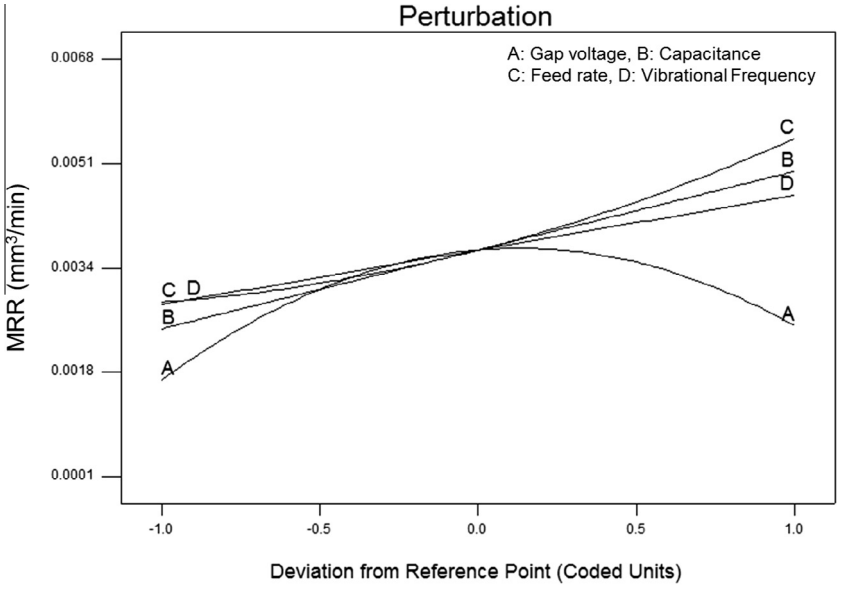

Fig. 6. Perbutation plot for MRR.

by capacitor is released. The capacitance regulates the amount of the energy deposited and consequently, with increase in capacitance, the amount of DE, pulse current and pulse interval also increases boosting the MRR [30]. Therefore, the MRR increases prominently at high values of capacitance. The similar observation regarding increase of MRR with increase in DE also reported by [2,12]. The increase of MRR with increase in vibrational frequency (Fig. 6) values can be explained with considering adhesion effect. In micro-EDM, the adhesion between electrode and workpiece plays important role on machining performance. Frequent shorts circuits occurs due to adhesion and when short circuit occurs, machine pullbacks the electrode opposite to feed direction to maintain the spark gap [34]. Due to vibrational frequency, the workpiece vibrates and the adhesion between electrode and workpiece recovered effectively. Moreover, the vibrational movement of workpiece leads to effective evacuation of debris and molten metal from machining zone due to turbulent flow of dielectric in machining zone.

3.3. Analysis of kerf

Fig. 8 shows the perturbation plot for kerf width. The kerf width is observed to be more sensitive to capacitance followed by gap voltage as compared feed rate and vibrational frequency. The capacitance and gap voltage lines are steep than the flat lines for feed rate and vibrational frequency. The kerf width increases with an increase in both gap voltage as well as capacitance values. The similar observation also reported by [11,12,34]. For achieving, lower kerf width, the low discharge energy values (i.e. low gap voltage and low capacitance) are suitable. The kerf width increases at high discharge energy due to the quantum electrons released from negative wire electrode striking with neutral particles in

Please cite this article in press as: D.R. Unune, H.S. Mali, Experimental investigation on low-frequency vibration assisted micro-WEDM of Inconel 718, Eng. Sci. Tech., Int. J. (2016), http://dx.doi.org/10.1016/j.jestch.2016.06.010

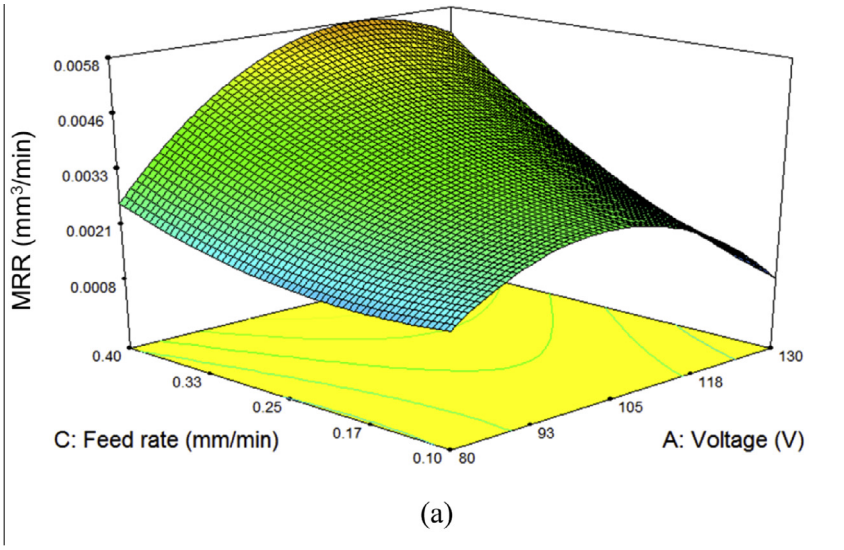

(a)

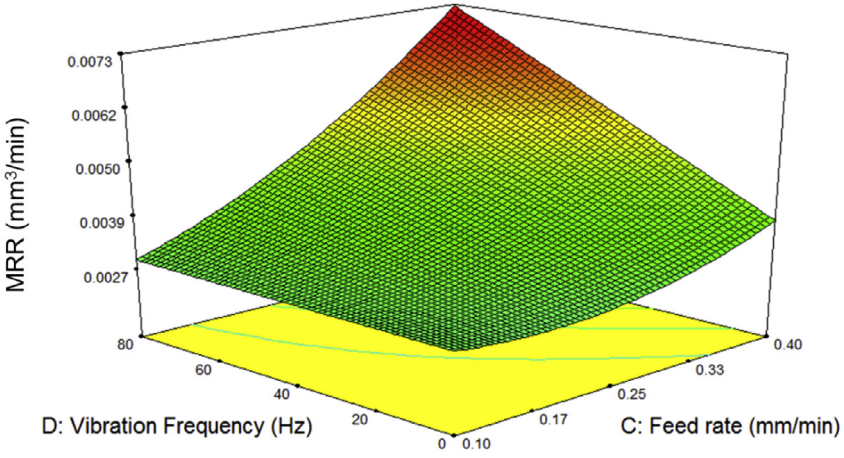

(b)

Fig. 7. Response graphs for MRR.

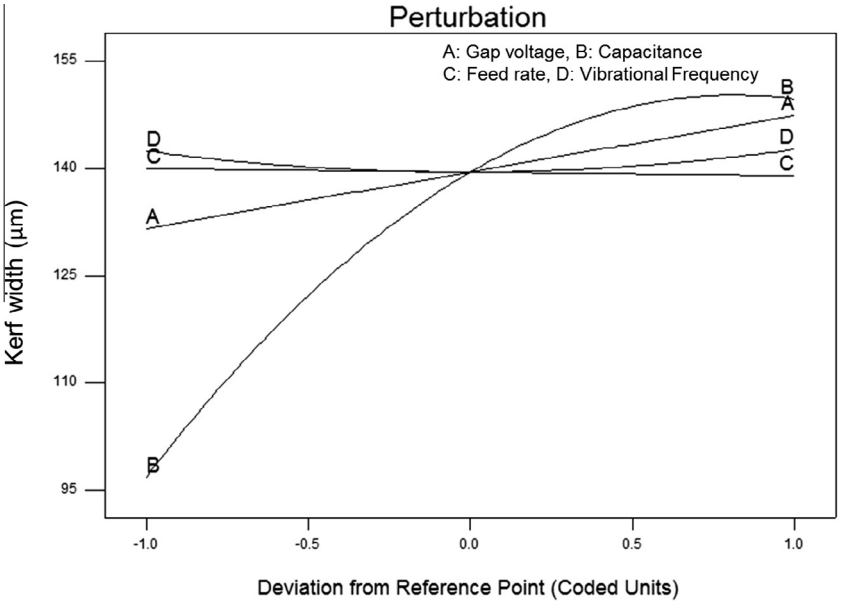

Fig. 8. Perbutation plot for kerf width.

Please cite this article in press as: D.R. Unune, H.S. Mali, Experimental investigation on low-frequency vibration assisted micro-WEDM of Inconel 718, Eng. Sci. Tech., Int. J. (2016), http://dx.doi.org/10.1016/j.jestch.2016.06.010

Table 5
Comparison of micro-WEDM with and without low-frequency vibration assistance.

Sr. No.	Control factors			Performance measures					
	Voltage (V)	Capacitance (μF)	Feed rate (mm/min)	MRR (mg/min)			Kerf width (μm)		
				Without vibration	With vibration (80 Hz)	% improvement	Without vibration	With vibration (80 Hz)	% improvement
1	105	0.01	0.25	0.0016407	0.0030686	87.02	101	98	−2.97
2	80	0.1	0.25	0.0034219	0.0057769	68.82	111	113	1.80
3	105	0.1	0.4	0.0036652	0.0057949	58.10	129	121	−6.20
4	105	0.1	0.1	0.0011712	0.0018346	56.64	123	129	4.88
5	130	0.1	0.25	0.0012259	0.0019451	58.66	128	134	4.69
6	105	0.4	0.25	0.0036114	0.0060655	67.95	155	153	−1.29

the dielectric fluids, which results in larger ionization effect. The kerf width will increase when a large amount of electrodes and ions strikes with the workpiece [11,34]. The machining at low discharge energy will enhance the dimensional accuracy and reduction of radius while cutting a corner in micro-machined components.

3.4. Comparison of with and without vibration assisted micro-WEDM

For the comparison of the performance of micro-WEDM with and without low-frequency vibration assistance, the experiments at same settings of gap voltage, capacitance, and feed rate while at with and without vibration condition are chosen and listed separately in Table 5. The performance measure values in experiment number 3,6,11,12,14,19,21,22,24,25,28,29 are compared and the percentage improvement in performance measures is calculated using following equation;

$$\text{Percentage improvement in performance measure} = \frac{\text{Performance measure value with vibration} - \text{Performance measure value without vibration}}{\text{Performance measure value without vibration}} \times 100\% \quad (4)$$

The maximum percentage improvement in MRR is observed to be 87.02% at low discharge energy settings. It has been noted that the mean percentage improvement for MRR is 66.20% pointing that low-frequency vibration assistance enhances the machining condition in micro-WEDM and thereby improves the MRR of micro-WEDM. It has been observed that vibration does not affect the kerf width significantly. The maximum percentage increase in kerf width is noted to be 4.88%. The mean percentage improvement for kerf width is observed to be 0.15%.

3.5. Microscopic investigation of surface topography of micro-channels

The surface topographical images of microchannels fabricated by micro-WEDM in Inconel 718 are shown in Fig. 9. The effects different energy settings viz. 320 μJ and 2205 μJ on channel surface are shown in Fig. 9(a) and (b), respectively. It is observed that in micro-WEDM, the surface morphology depends on the applied discharge energy while machining. At low discharge energy setting, the machined surface observed to be very smooth. However, at high discharge energy settings, the spherical debris/globules and larger resolidified layer is observed on the machined surface. The formation of spherical debris/globules occurs rapid cooling and quenching of vaporized metal or splashed molten metal. At low discharge energy, the shape of the microchannel is observed to be more accurate as compared to microchannel at high discharge

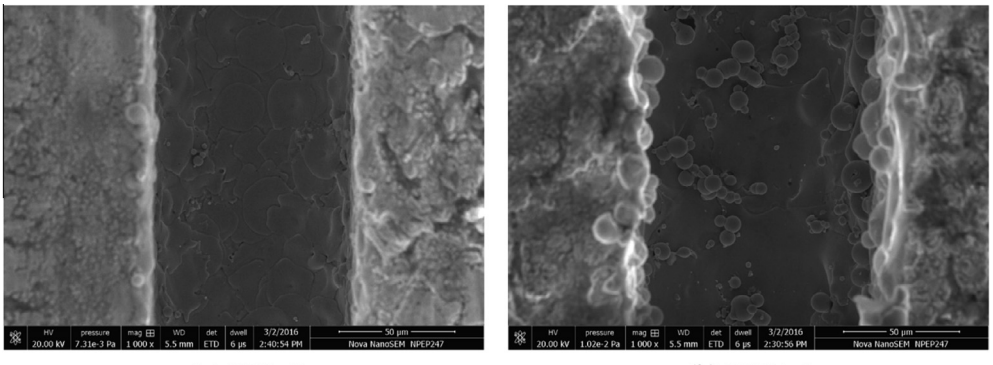

Fig. 9. Scanning electron microscope images of microchannels at different energy settings.

Please cite this article in press as: D.R. Unune, H.S. Mali, Experimental investigation on low-frequency vibration assisted micro-WEDM of Inconel 718, Eng. Sci. Tech., Int. J. (2016), http://dx.doi.org/10.1016/j.jestch.2016.06.010

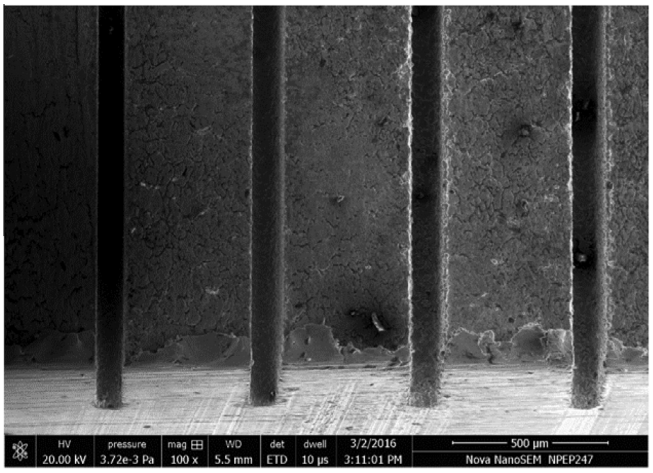

Fig. 10. Micro-channels fabricated using micro-WEDM in Inconel 718.

energy. Fig. 10 shows micro-channels formed in Inconel 718 using micro-WEDM process.

4. Conclusion

In this work, an attempt was made to perform micro-WEDM with low-frequency workpiece vibration assistance. The Box–Behnken design was used to design the experiments considering gap voltage, capacitance, feed rate and vibrational frequency as control factors while MRR and kerf width as performance measures. From the experimental and statistical analysis, the following conclusions were drawn:

- The empirical model developed for low-frequency vibration assisted micro-WEDM of Inconel 718 and are given below:

$$\begin{aligned}\text{MRR} = {} & -0.22818 + (5.15586 \times 10^{-4})\text{A} + (6.4794 \times 10^{-3})\text{B} \\ & - (0.032039)\text{C} - (1.42332 \times 10^{-5})\text{D} + (2.32532 \times 10^{-4})\text{AD} \\ & + (1.44429 \times 10^{-4})\text{CD} - 2.6488\text{B}^2 + 0.021177\text{C}^2\end{aligned}$$

$$\begin{aligned}\text{Kerf width} = {} & +58.55654 + 0.31572\text{A} + 310.69223\text{B} + 19.95333\text{C} \\ & - (-4.47727 \times 10^{-3})\text{D} - 0.58333\text{CD} \\ & - 426.95416\text{B}^2 + (1.91534 \times 10^{-3})\text{D}^2\end{aligned}$$

- The capacitance was observed to be a predominant factor influencing both MRR and kerf width and contributes by 26.38% and 87.47%, respectively. Both MRR and kerf width increases with increase in capacitance.
- ANOVA test recognized gap voltage (A), capacitance (B), feed rate (C), vibrational frequency (D), interaction between gap voltage and feed rate (AC), interaction between feed rate and vibrational frequency (CD), and pure quadratic effect of gap voltage and feed rate have significant influence on MRR of micro-WEDM of Inconel 718. The kerf is affected significantly by gap voltage, capacitance, and quadratic effects of capacitance and vibrational frequency.
- It was observed that vibrational frequency contributes by 10.88% in MRR. In addition, the interaction between feed rate and vibrational frequency also contributes by 22.33% in MRR.
- From the comparison of the performance of micro-WEDM with and without vibration condition, it was noted that low-frequency vibration assistance improved the MRR by 66.20% as compared to without vibration assisted micro-WEDM.
- Overall, the low-frequency vibration assistances improves the performance of the micro-WEDM due to enhanced the flushing conditions and reduced electrode-workpiece adhesion.

The low-frequency vibration found effective in improving process performance of μ-WEDM, though, further investigations are necessary in term of accuracy of fabricated micro-features, form, and shape of fabricated micro-feature, effects of vibrations frequency on surface topography of machined surfaces.

References

[1] D. Zhu, X. Zhang, H. Ding, Tool wear characteristics in machining of nickel-based superalloys, Int. J. Mach. Tools Manuf. 64 (2013) 60–77.
[2] V. Aggarwal, S.S. Khangura, R.K. Garg, Parametric modeling and optimization for wire electrical discharge machining of Inconel 718 using response surface methodology, Int. J. Adv. Manuf. Technol. 79 (1–4) (2015) 31–47.
[3] M. Nalbant, A. Altın, H. Gökkaya, The effect of cutting speed and cutting tool geometry on machinability properties of nickel-base Inconel 718 super alloys, Mater. Des. 28 (4) (2007) 1334–1338.
[4] W. Akhtar, J. Sun, P. Sun, W. Chen, Z. Saleem, Tool wear mechanisms in the machining of Nickel based super-alloys: a review, Front. Mech. Eng. 9 (2) (2014) 106–119.
[5] S. Pervaiz, A. Rashid, I. Deiab, M. Nicolescu, Influence of tool materials on machinability of titanium- and nickel-based alloys: a review, Mater. Manuf. Process. 29 (3) (2014) 219–252.
[6] R. Chalisgaonkar, J. Kumar, Multi-response optimization and modeling of trim cut WEDM operation of commercially pure titanium (CPTi) considering multiple user's preferences, Eng. Sci. Technol. Int. J. 18 (2) (2015) 125–134, http://dx.doi.org/10.1016/j.jestch.2014.10.006.
[7] N. Sharma, R. Khanna, R.D. Gupta, WEDM process variables investigation for HSLA by response surface methodology and genetic algorithm, Eng. Sci. Technol. Int. J. 18 (2) (2015) 171–177, http://dx.doi.org/10.1016/j.jestch.2014.11.004.
[8] S.S. Mahapatra, A. Patnaik, Optimization of wire electrical discharge machining (WEDM) process parameters using Taguchi method, Int. J. Adv. Manuf. Technol. 34 (9–10) (2006) 911–925.
[9] M.P. Jahan, M. Rehman, Y.S. Wong, Micro-electrical discharge machining (Micro-EDM), in: H.G. Saleem (Ed.), Comprehensive Materials Processing, Elsevier, Oxford, 2014, pp. 333–371.
[10] K.H. Ho, S.T. Newman, S. Rahimifard, R.D. Allen, State of the art in wire electrical discharge machining (WEDM), Int. J. Mach. Tools Manuf. 44 (12–13) (2004) 1247–1259.
[11] B. Kuriachen, K.P. Somashekhar, J. Mathew, Multiresponse optimization of micro-wire electrical discharge machining process, Int. J. Adv. Manuf. Technol. 76 (1–4) (2014) 91–104.
[12] P. Sivaprakasam, P. Hariharan, S. Gowri, Modeling and analysis of micro-WEDM process of titanium alloy (Ti–6Al–4V) using response surface approach, Eng. Sci. Technol. Int. J. 17 (4) (2014) 227–235, http://dx.doi.org/10.1016/j.jestch.2014.06.004.
[13] D. Kondayya, A. Gopala Krishna, An integrated evolutionary approach for modelling and optimization of wire electrical discharge machining, Proc. Inst. Mech. Eng. Part B J. Eng. Manuf. 225 (4) (2011) 549–567.
[14] K. Kumar, S. Agarwal, Multi-objective parametric optimization on machining with wire electric discharge machining, Int. J. Adv. Manuf. Technol. 62 (5–8) (2011) 617–633.
[15] S. Kuriakose, K. Mohan, M.S. Shunmugam, Data mining applied to wire-EDM process, J. Mater. Process. Technol. 142 (1) (2003) 182–189.
[16] S. Sarkar, S. Mitra, B. Bhattacharyya, Parametric analysis and optimization of wire electrical discharge machining of γ-titanium aluminide alloy, J. Mater. Process. Technol. 159 (3) (2005) 286–294, http://dx.doi.org/10.1016/j.jmatprotec.2004.10.009.
[17] A. Manna, B. Bhattacharya, Taguchi and Gauss elimination method: a dual response approach for parametric optimization of CNC wire cut EDM of PR Al SiC MMC, Int. J. Adv. Manuf. Technol. 28 (2006) 67–75.
[18] N.G. Patil, P.K. Brahmankar, Some studies into wire electro-discharge machining of alumina particulate-reinforced aluminum matrix composites, Int. J. Adv. Manuf. Technol. 48 (5–8) (2009) 537–555.
[19] R. Bobbili, V. Madhu, A.K. Gogia, Modelling and analysis of material removal rate and surface roughness in wire-cut EDM of armour materials, Eng. Sci. Technol. Int. J. 18 (4) (2015) 664–668, http://dx.doi.org/10.1016/j.jestch.2015.03.014.
[20] R. Bobbili, V. Madhu, A.K. Gogia, Multi response optimization of wire-EDM process parameters of ballistic grade aluminium alloy, Eng. Sci. Technol. Int. J. 18 (4) (2015) 720–726, http://dx.doi.org/10.1016/j.jestch.2015.05.004.
[21] F. Han, G. Cheng, Z. Feng, S. Isago, Thermo-mechanical analysis and optimal tension control of micro wire electrode, Int. J. Mach. Tools Manuf. 48 (7–8) (2008) 922–931.
[22] S. Das, S.S. Joshi, Modeling of spark erosion rate in microwire-EDM, Int. J. Adv. Manuf. Technol. 48 (5–8) (2009) 581–596, http://dx.doi.org/10.1007/s00170-009-2315-1.

Please cite this article in press as: D.R. Unune, H.S. Mali, Experimental investigation on low-frequency vibration assisted micro-WEDM of Inconel 718, Eng. Sci. Tech., Int. J. (2016), http://dx.doi.org/10.1016/j.jestch.2016.06.010

[23] M.T. Yan, An adaptive control system with self-organizing fuzzy sliding mode control strategy for micro wire-EDM machines, Int. J. Adv. Manuf. Technol. 50 (1-4) (2009) 315–328, http://dx.doi.org/10.1007/s00170-009-2481-1.

[24] D.R. Unune, H.S. Mali, Artificial neural network–based and response surface methodology–based predictive models for material removal rate and surface roughness during electro-discharge diamond grinding of Inconel 718, Proc. Inst. Mech. Eng. Part B J. Eng. Manuf. (2015), http://dx.doi.org/10.1177/0954405415619347.

[25] A. Goswami, J. Kumar, Optimization in wire-cut EDM of Nimonic-80A using Taguchi' approach and utility concept, Eng. Sci. Technol. Int. J. 17 (2014) 664–668, http://dx.doi.org/10.1016/j.jestch.2014.07.001.

[26] M.S. Hewidy, T.A. El-Taweel, M.F. El-Safty, Modelling the machining parameters of wire electrical discharge machining of Inconel 601 using RSM, J. Mater. Proc. Technol. 169 (2) (2005) 328–336.

[27] R. Ramakrishnan, L. Karunamoorthy, Modeling and multi-response optimization of Inconel 718 on machining of CNC WEDM process, J. Mater. Proc. Technol. 207 (1–3) (2008) 343–349.

[28] R. Ramakrishnan, L. Karunamoorthy, Performance studies of wire electro discharge machining (WEDM) of Inconel 718, Int. J. Mater. Prod. Technol. 35 (1–2) (2009) 199–215, http://dx.doi.org/10.1504/IJMPT.2009.025227.

[29] B.B. Nayak, S.S. Mahapatra, Optimization of WEDM process parameters using deep cryo-treated Inconel 718 as work material, Eng. Sci. Technol. Int. J. 19 (1) (2016) 61–170, http://dx.doi.org/10.1016/j.jestch.2015.06.009.

[30] M.P. Jahan, M. Rahman, Y.S. Wong, L. Fuhua, On-machine fabrication of high-aspect-ratio micro-electrodes and application in vibration-assisted micro-electrodischarge drilling of tungsten carbide, Proc. Inst. Mech. Eng. Part B J. Eng. Manuf. 224 (5) (2010) 795–814.

[31] M.P. Jahan, Y.S. Wong, M. Rahman, Evaluation of the effectiveness of low frequency workpiece vibration in deep-hole micro-EDM drilling of tungsten carbide, J. Manuf. Processes 14 (3) (2012) 343–359.

[32] P.A. Lee, Y. Kim, B.H. Kim, Effect of low frequency vibration on micro EDM drilling, Int. J. Precis. Eng. Manuf. 16 (13) (2015) 2617–2622.

[33] D.R. Unune, H.S. Mali, Current status and applications of hybrid micro-machining processes: a review, Proc. Inst. Mech. Eng. Part B J. Eng. Manuf. 229 (10) (2014) 1681–1693.

[34] K.P. Somashekhar, N. Ramachandran, J. Mathew, Material removal characteristics of microslot (kerf) geometry in μ-WEDM on aluminum, Int. J. Adv. Manuf. Technol. 51 (5–8) (2010) 611–626.

Please cite this article in press as: D.R. Unune, H.S. Mali, Experimental investigation on low-frequency vibration assisted micro-WEDM of Inconel 718, Eng. Sci. Tech., Int. J. (2016), http://dx.doi.org/10.1016/j.jestch.2016.06.010